A new formulation of total unsharpness in radiography

PHYS. MED. BIOL., 1977, VOL. 22, NO. 1, 70–80.

A New Formulation of Total Unsharpness in Radiography

A. A. HARMS† and A. ZEILINGER

Atominstitut der Österreichischen Hochschulen, A-1020, Vienna, Austria

Received 12 *March* 1976

ABSTRACT. A new formulation of total unsharpness in radiography based on line spread and edge spread function analysis is established and investigated. The unsharpness contributions due to (1) screen conversion, (2) object motion and (3) geometric effects are incorporated into a general integral formulation. Comparisons with experiments are undertaken and the ambiguity, as well as limitation, of a widely used empirical unsharpness formula is clarified.

1. Introduction

Spiegler and Norman (1973) have re-emphasized the state of ambiguity and confusion which exists concerning the correct analytical representation of the total unsharpness in radiography. Basically, the problem involves both the form of the function and the magnitude of the exponent in the empirical total unsharpness formula

$$U_t = (U_g^n + U_m^n + U_s^n)^{1/n}. \tag{1}$$

Here U_g is the geometric unsharpness, U_m is the motion unsharpness and U_s is the screen unsharpness. Historically, values of $n = 1$, 2 and 3 have been proposed by Bouwers (1936), Newell (1938) and Klasens (1946) respectively. Although the above empirical formula is widely used, numerous textbook authors have expressed both disquiet and caution about the use of the above formula (Seeman 1968, Herz 1969, Christensen, Curry and Nunnally 1972).

The purpose of this analysis is to develop an alternative—and we believe a more correct—formulation regarding the total unsharpness in radiography. The analytical and conceptual foundation is based on both physical and mathematical plausibility arguments. In addition, recourse to experimental results will be made and suggestions for its application will be introduced.

2. Functional analysis

As our starting point we consider the experimentally obtainable film optical density associated with an ideal radiation-absorbing knife-edge object as illustrated in fig. 1. Of specific interest is the trace of a microdensitometer across the edge of the image which we assume to be smoothed to represent a statistically reproducible monotonically increasing S-shaped optical density function; we will call this the edge spread function (ESF) and symbolically represent it by $S(x, \alpha)$. Here, as suggested in fig. 1, x is the position variable

† Permanent address: Department of Engineering Physics, McMaster University, Hamilton, Ontario, Canada.

referenced to zero at the perpendicular coordinate of the knife-edge object and $\boldsymbol{\alpha}$ is a vector composed of suitable systems parameters such as film type, energy of source, etc. For convenience and generality we assume that the ESF, $S(x, \boldsymbol{\alpha})$, is suitably normalized to the asymptotes to yield $S(-\infty, \boldsymbol{\alpha}) = 0$, and $S(+\infty, \boldsymbol{\alpha}) = 1$ (fig. 1).

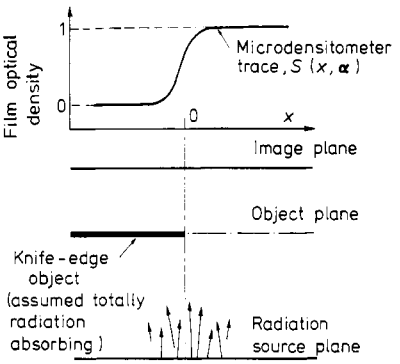

Fig. 1. Schematic representation of a radiographic imaging system illustrating main component and film optical density associated with a knife-edge object.

We may relate the edge spread function, ESF, to the line spread function (LSF), $L(x, \boldsymbol{\alpha})$ (Spiegler and Norman 1973), by the dual integral–differential relations of

$$L(x, \boldsymbol{\alpha}) = N \frac{\partial}{\partial x} S(x, \boldsymbol{\alpha}) \tag{2}$$

or

$$S(x, \boldsymbol{\alpha}) = N^{-1} \int_{-\infty}^{x} L(\xi, \boldsymbol{\alpha}) \, \mathrm{d}\xi \tag{3}$$

where N is a normalization factor as required.

Either the ESF or the LSF could be used to define an unsharpness of the optical image of the knife-edge object, fig. 1. We note that in practice the ESF will be relatively smooth without discontinuities; indeed a sharp discontinuity could develop only in the limit of an idealized geometric unsharpness in the total absence of screen and motion unsharpness. Thus, the relative smoothness of the ESF and the continuity of its first derivative is a reasonable assumption to make. A definition of unsharpness, accepted by convention, is thus required. We will consider several possibilities and will make clear that our subsequent analysis may be adapted to either of these definitions.

3. Definitions of unsharpness

The practising radiographer may find a definition of unsharpness based on visual discrimination most convenient. For example, the 10–90% toe-and-heel coordinate of the ESF could be used to give the unsharpness in units of length.

If we therefore choose x_1 and x_2 by the conditions

$$S(x_1, \boldsymbol{\alpha}) = 0{\cdot}1 \quad \text{and} \quad S(x_2, \boldsymbol{\alpha}) = 0{\cdot}9 \tag{4}$$

then the unsharpness is given by

$$U = x_2 - x_1. \tag{5}$$

A mathematically convenient definition may be the inverse of the slope of the ESF at the point of inflection x_0:

$$U = \left[\frac{\partial}{\partial x} S(x, \boldsymbol{\alpha})|_{x_0}\right]^{-1}. \tag{6}$$

Or, if the optical density variation near the asymptotes is of particular importance, choose a convenient value for $S(x_1, \boldsymbol{\alpha})$ and $S(x_2, \boldsymbol{\alpha})$ to define x_1 and x_2 and use

$$U = \frac{x_2 - x_1}{S(x_2, \boldsymbol{\alpha}) - S(x_1, \boldsymbol{\alpha})}. \tag{7}$$

Further, in view of the unambiguous relationship between the ESF and LSF, eqn (2) and eqn (3), we could use the full-width-at-half-maximum of the LSF; that is

$$U = x_2^0 - x_1^0 \tag{8}$$

where x_1^0 and x_2^0 are chosen by the condition

$$L(x_1^0, \boldsymbol{\alpha}) = L(x_2^0, \boldsymbol{\alpha}) = \tfrac{1}{2} L(x, \boldsymbol{\alpha})_{\max}. \tag{9}$$

Finally, we mention the possibility of the standard deviation of the LSF as a suitable unsharpness definition:

$$U = \left[\int_{-\infty}^{\infty} (x - \bar{x})^2 L(x, \boldsymbol{\alpha})\, \mathrm{d}x\right]^{\frac{1}{2}}. \tag{10}$$

In listing the above possible definitions of unsharpness, we do not wish to promote one of the definitions over all others; the matter of convenience of use will obviously decide that question; we do, however, wish to emphasize the need for consistency in the use of unsharpness in presenting analytical and experimental results. The alternative, of course, is the full representation of the ESF, or LSF, which we will consider shortly.

4. Components of unsharpness

We refer to fig. 1 to emphasize the physical-geometric system of interest and consider fig. 2(*a*) as one special case: a stationary knife-edge object and collimated beam of radiation. Clearly, in this case both geometric and motion unsharpness are zero and therefore, for this case, we define the ESF by

$$S_s(x, \boldsymbol{\alpha}) = \text{ESF associated with screen unsharpness only.} \tag{11}$$

The subscript s is used to identify the effect due to screen unsharpness.

We now consider the above case but modify the radiation source to produce a geometric unsharpness effect. Specifically, we consider a slit of width a of isotropic radiation in the source plane, fig. 2(*b*). A geometric unsharpness parameter μ is introduced in the usual manner

$$\mu = \frac{al}{L} \tag{12}$$

where l is the object-to-image distance and L is the source-to-object distance.

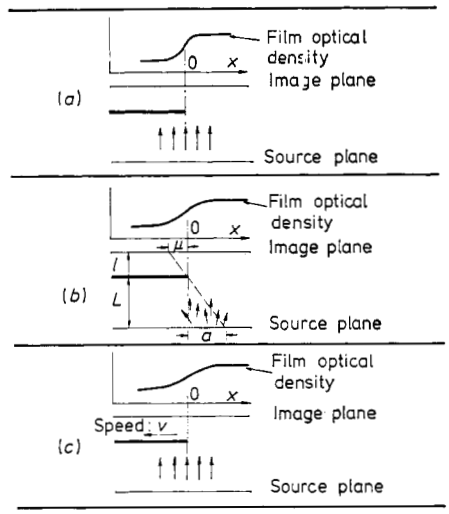

Fig. 2. System characteristics associated with (*a*) screen unsharpness, (*b*) geometric unsharpness and (*c*) motion unsharpness.

Clearly, then, the combined unsharpness effect of both screen conversion and the geometric condition on the resultant ESF is now given in integral form as

$$S_{s,g}(x, \mu, \alpha) = \frac{1}{\mu} \int_{x'=0}^{\mu} S_s(x + x', \alpha)\, dx' \tag{13}$$

where the subscripts (s, g) are used to indicate the combined screen and geometric unsharpness contribution. Note that this ESF represents an integral relationship between the screen and geometric unsharpness rather than an independent additive relation as provided by the empirical formula, eqn (1). We note in passing that if the radiation source were not isotropic then a weighting function $\rho(x')$ would need to be included in the integral, eqn (13).

Returning to the case of a collimated beam of radiation, we allow the knife-edge object to move in the negative-x direction with a speed v while the exposure time is τ (fig. 2(*c*)). The resultant ESF, now including both screen and motion unsharpness effects, is given by

$$S_{s,m}(x, v, \tau, \alpha) = \frac{1}{\tau} \int_{0}^{\tau} S_s(x + |v|\tau, \alpha)\, dt. \tag{14}$$

Combining the three independent effects—screen, geometry and motion—and assuming a non-isotropic radiation source, yields an ESF given in general form by

$$S_{s,m,g}(x, v, \tau, \mu, \alpha) = \frac{1}{\mu\tau} \int_{x'=0}^{\mu} \int_{t=0}^{\tau} \rho(x')\, S_s(x + x' + |v|\, t, \alpha)\, dt\, dx'. \qquad (15)$$

Thus, for the complete and correct evaluation of the total image unsharpness it is only necessary to integrate the appropriate ESF, $S_s(x, \alpha)$. We now consider the specification of such a function.

5. Edge spread function representation

We follow the common practice of identifying a physically plausible LSF and from it obtain the ESF according to eqn (3). In fig. 3 we show graphically four potential candidates based on their relevance in related studies: (1) rectangular,

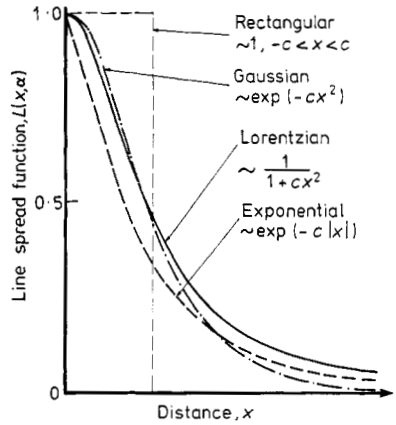

Fig. 3. Schematic and analytical representation of four line spread functions (LSF).

(2) Gaussian, (3) Lorentzian and (4) exponential; their corresponding functional representations are also shown in the same figure. By visual comparison with the exacting experimentally obtained X-ray data as reported by Rossmann, Lubberts and Cleare (1964) we reject the rectangular function as too gross an approximation. The Gaussian function is too large near the origin and too shallow in the wings. Both the Lorentzian—which has been found very useful in spectroscopy (Shore and Menzel 1968) and in neutron radiography (Harms, Garside and Chan 1972)—and the exponential previously used by Rossmann *et al.* (1964) provide a reasonably good fit depending upon the range of x chosen; numerical curve fitting has shown that the Lorentzian can provide a better fit with experimental data for x close to zero while the exponential seems to fit better for larger values of $\pm x$. We have chosen to adopt the Lorentzian, rather than the exponential, for the following reasons:

(*a*) The exponential provides a physically unreal representation at $x = 0$ by virtue of the non-existence of a slope at this point; we point out that the Rossmann *et al.* (1964) experimental data show a zero slope at $x = 0$.

(*b*) The major contribution of the LSF comes from the domain of x close to zero.

Thus, the ESF for the screen conversion process to be used in our subsequent analysis is given by eqn (3):

$$S_s(x,c) = N\int_{-\infty}^{x}\frac{1}{1+c\xi^2}\,d\xi = \frac{1}{2}+\frac{1}{\pi}\tan^{-1}(x\sqrt{c}) \tag{16}$$

where the normalization factor N has been so chosen to give $S_s(x,c)\to\{0,1\}$ as $x\to\{-\infty,+\infty\}$. Also, the systems vector $\boldsymbol{\alpha}$ is fully defined by one systems parameter c. This dispersion parameter can be readily obtained by curve fitting eqn (16) to an experimentally obtained knife-edge image scan for the

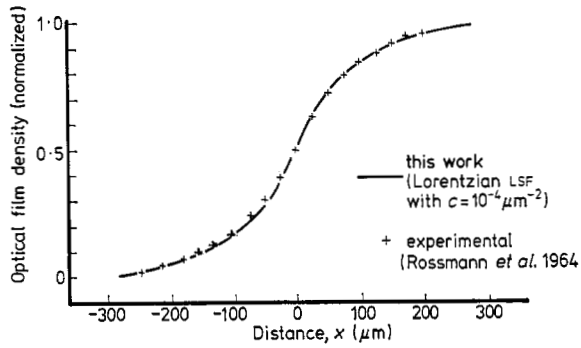

Fig. 4. Comparison between experimental optical density data and the Lorentzian edge spread function: screen unsharpness effect only, $S_s(x,c)$.

case of a stationary knife-edge object with a highly collimated radiation beam and having the object sufficiently close to the film to eliminate geometric unsharpness contributions. Clearly, it is expected that c will vary with film emulsion used, type—if any—of intensifying screen, and in addition may exhibit a dependence on radiation energy. Thus, it is a constant of the radiographic system.

In fig. 4 we show a comparison between the Lorentzian ESF, eqn (16), with the published experimental data of Rossmann *et al.* (1964); the dispersion parameter used was $c = 10^{-4}\ \mu m^{-2}$ and the data was normalized to zero and unity at $\pm 280\ \mu m$. Similar agreement for other screen–film combinations in neutron radiography has been found (Harms *et al.* 1975). The fit between the Lorentzian ESF and the experimental data is clearly very good and seems to justify its wider use in radiography.

The ESF which incorporates both screen and geometric effects, eqn (13), is now, with the use of eqn (16), given by

$$\begin{aligned} S_{s,g}(x,\mu,c) &= \frac{1}{\mu}\int_{x'=0}^{\mu}\left\{\frac{1}{2}+\frac{1}{\pi}\tan^{-1}[\sqrt{c}(x+x')]\right\}dx' \\ &= \frac{1}{2}+\frac{1}{\pi}\left\{\tan^{-1}[\sqrt{c}(x+\mu)]+\frac{x}{\mu}\{\tan^{-1}[\sqrt{c}(x+\mu)]-\tan^{-1}(x\sqrt{c})\}\right. \\ &\quad \left.+\frac{1}{2\mu\sqrt{c}}\left[\ln\left(\frac{1+cx^2}{1+c(x+\mu)^2}\right)\right]\right\}. \end{aligned} \tag{17}$$

We observe that this screen-geometric effect ESF retains the characteristic symmetry and asymptotes of the screen ESF of eqn (16) as $|x| \gg \mu$.

The corresponding ESF for the case of screen and motion effects is given in an analogous manner,

$$S_{s,m}(x, v, \tau, c) = \frac{1}{\tau}\int_{t-0}^{\tau}\left\{\frac{1}{2}+\frac{1}{\pi}\tan^{-1}[(\sqrt{c}(x+vt)]\right\}dt$$

$$= \frac{1}{2}+\frac{1}{\pi}\left\{\tan^{-1}[\sqrt{c}(x+v\tau)]+\frac{x}{v\tau}\{\tan^{-1}[\sqrt{c}(x+v\tau)]-\tan^{-1}(x\sqrt{c})\}\right.$$

$$\left.+\frac{1}{2v\tau\sqrt{c}}\left[\ln\left(\frac{1+cx^2}{1+c(x+v\tau)^2}\right)\right]\right\}. \tag{18}$$

We note that the algebraic form of eqn (18) is equivalent to that of eqn (17) with μ being replaced by $v\tau$.

The ESF which incorporates all three unsharpness contributions—screen, geometric and motion—follows by an integration of either eqn (17) over $t \in (0, \tau)$ or of eqn (18) over $x' \in (0, \mu)$. However, these integrations lead to functionally intractable and numerically cumbersome expressions and would clearly represent an inconvenience if they had to be performed every time a radiograph with a different set of c, μ and $v\tau$ were examined. It is clear though that a computer calculation of tables of unsharpness, based on one or two of the suggested definitions, could readily be accomplished and appropriately circulated. These tables—or graphical representations thereof—could be reasonably compact since only three independent variables are involved: c, μ and $v\tau$. Thus, in principle this new formulation of image sharpness could be incorporated into the practice of radiography.

We now wish to develop some useful generalizations and extensions on radiographic image unsharpness based on the methodology suggested here.

6. Generalizations and extensions

As we indicated previously, the two ESF for screen-geometry effect, eqn (17), and screen-motion effects, eqn (18), are functionally identical. We define therefore

$$U_{g/m} = \begin{cases} \mu = al/L, & \text{if no motion unsharpness exists} \\ v\tau, & \text{if no geometric unsharpness exists.} \end{cases} \tag{19}$$

That is $U_{g/m}$ represents geometric unsharpness or motion unsharpness but not the sum of both; this latter point might be relaxed if the error introduced is acceptable. The substitution of $U_{g/m}$ in eqn (17) or eqn (18) makes it apparent that if we introduce a linearly transposed position variable

$$x^* = x + \frac{U_{g/m}}{2} \tag{20}$$

and define

$$x_+ = \sqrt{(c)}\left(x^* + \frac{U_{g/m}}{2}\right) \tag{21a}$$

$$x_- = \sqrt{(c)}\left(x^* - \frac{U_{g/m}}{2}\right). \tag{21b}$$

Then the transposed ESF which incorporates either screen-geometry or screen-motion unsharpness is given in a symmetric form with respect to x_+ and x_-

$$S(x^*, U_{g/m}, c) = \frac{1}{2} + \frac{1}{\pi}\left\{\frac{1}{2}(\tan^{-1}x_+ + \tan^{-1}x_-) + \frac{x^*}{U_{g/m}}(\tan^{-1}x_+ - \tan^{-1}x_-)\right.$$
$$\left. - \frac{1}{2U_{g/m}}\sqrt{c}\left[\ln\left(\frac{1+x_+^2}{1+x_-^2}\right)\right]\right\}. \tag{22}$$

This transposed ESF possesses the property of reflection

$$-S(-x^*, U_{g/m}, c) = S(x^*, U_{g/m}, c), \tag{23}$$

normalized summation

$$S(x^*, U_{g/m}, c) + S(-x^*, U_{g/m}, c) = 1 \tag{24}$$

and a point of inflection at $x^* = 0$, that is at $x = -U_{g/m}/2$.

We show some interesting properties of the ESF in fig. 5 where, for clarity of presentation, the dispersion parameter has been set to $c = 1$. For $U_{g/m}$ small,

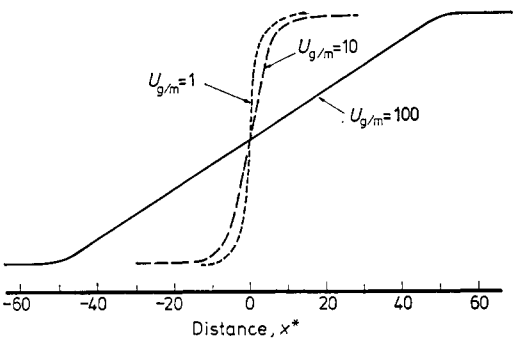

Fig. 5. Change in the edge spread function (ESF) with increasing geometric or motion unsharpness; $U_{g/m}$ and x^* are in units of $1/\sqrt{c}$.

fig. 5, the ESF shows the smooth shape associated with the specialized experimental data of Rossmann *et al.* (1964), fig. 4 and eqn (16). As $U_{g/m}$ increases, however, an increasingly pronounced linear domain about $x^* = 0$ becomes evident, fig. 5. This trend is physically obvious: with c = constant, the screen unsharpness is constant, and as $U_{g/m}$ increases the geometric unsharpness or motion unsharpness became more dominant and linear by virtue of eqn (19). The screen unsharpness contributes to smoothing the curve at the corners which is particularly apparent for $U_{g/m} = 100$.

7. Correlation with the empirical unsharpness formula

As developed herein, eqns (16), (17) and (18) are viewed as providing the more correct description of image sharpness in radiography. We wish to use these representations and relate them to the empirical unsharpness formula, eqn (1). Specifically we wish to enquire, as Spiegler and Norman (1973) did, about the choice of the exponent n in eqn (1) under conditions of a specific definition of unsharpness.

In an initial observation we point out that whenever one of U_g, U_m or U_s in eqn (1) dominates, that is it is significantly larger than the other(s), then the choice of exponent is irrelevant because

$$U_t \simeq (U_j^n)^{1/n} \tag{25}$$

for any positive n with j being one of g, m or s. Indeed, it is most important to have a correct value of n whenever the unsharpness components U_g, U_m and U_s are of similar magnitude. As our operational definition for the total unsharpness we choose to use the inverse slope, eqn (6), and hence using eqn (22) obtain

$$U_t = \frac{1}{(\partial S(x^*, U_{g/m}, c)/\partial x^*)}\bigg|x^* = 0 = \frac{\pi U_{g/m}}{2\tan^{-1}(U_{g/m}\sqrt{c}/2)}. \tag{26}$$

The screen unsharpness U_s is similarly obtained using eqn (16) since we require $U_{g/m} = 0$,

$$U_s = \frac{\pi}{\sqrt{c}}. \tag{27}$$

Dividing eqn (26) by eqn (27) permits the representation of unsharpness in dimensionless form as

$$\frac{U_t}{U_{gs}} = \frac{\pi U_{g/m}}{U_s\, 2\tan^{-1}(U_{g/m}\sqrt{c}/2)} = \frac{\pi U_{g/m}/U_s}{2\tan^{-1}[(\pi/2)(U_{g/m}/U_s)]}. \tag{28}$$

Thus we have U_t/U_s expressed as a function of $U_{g/m}/U_s$ within the context of the formalism developed here. Employing the empirical formula eqn (1) for screen and geometric unsharpness only leads to the companion expression

$$\frac{U_t}{U_s} = \left[1 + \left(\frac{U_g}{U_s}\right)^n\right]^{1/n}. \tag{29}$$

The comparison between eqn (28) and eqn (29) for $n = 1$, 2 and 3 is shown graphically in fig. 6 and clearly shows that neither of the three integer values of n is correct. Within the context of the unsharpness definition used here, eqn (26), the exponent n is greater than 1 but less than 2; indeed it is a function of the ratio U_g/U_s. We have evaluated this dependence by equating eqn (28) with eqn (29) and solved this transcendental equation by iteration. The results are shown in fig. 7 and clearly indicate this dependence. Thus, the empirical formula, eqn (1), could in principle still be used providing n is extracted from

fig. 7. As a rule of thumb we may suggest that, since the correct value of n is most important when

$$U_s \simeq U_g \tag{30}$$

then, by fig. 7, one should use

$$n \simeq 1{\cdot}55. \tag{31}$$

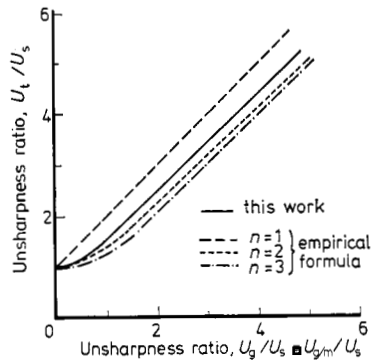

Fig. 6. Comparison of unsharpness ratios based on the use of the empirical formula for various n.

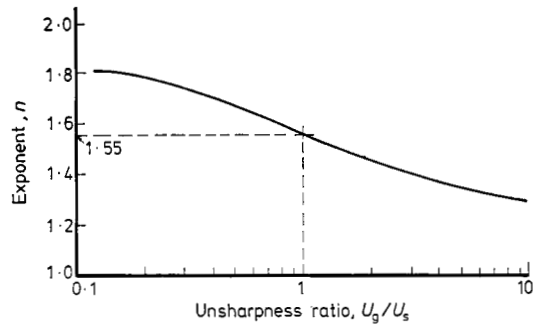

Fig. 7. Dependence of the exponent n in the empirical formula on the unsharpness ratio U_g/U_s.

8. Concluding comments

It is apparent that the exact specification of total unsharpness in radiography involves several analytical and numerical considerations. The most satisfying method would seem to be the specification of computer generated tables based on eqns (16), (17) and (18), as well as numerical integration of these last two equations. Since only three independent parameters are involved, c, μ and $v\tau$, it is clear that this could still be a most useful tabulation. The alternative is to use $n \simeq 1{\cdot}55$ recognizing that although it is an improvement over the historically used values of $n = 1$, 2 or 3, it is an average value and could be improved upon by calculating U_g/U_s and using fig. 7.

Résumé

Une nouvelle formulation de flou total en radiographie

On a établi et étudié une nouvelle formulation du flou total en radiographie, basée sur l'analyse des fonctions de propagations linéaire et marginale. Les contributions du flou dues à (1) la conversion sur écran, (2) les mouvements du sujet et (3) les effets géométriques sont incorporées dans une formulation intégrale générale. On a effectué des comparaisons avec des expériences, et l'ambiguité, ainsi que la limitation, d'une formule de flou empirique d'un emploi courant sont éclaircies.

Zusammenfassung

Eine neue Formulierung der totalen Unschärfe in der Radiographie.

Basierend auf einer Analyse der Linienverbreiterungen und Kantenverschmierungen wird eine neue Formulierung der totalen Unschärfe in der Radiographie vorgelegt und untersucht. In einer Integraldarstellung werden die einzelnen Beiträge zur Gesamtunschärfe aufgrund des (1) Konversionsprozesses, (2) der Bewegung des Objekts und (3) der geometrischen Effekte zusammengefasst. Vergleiche mit Experimenten werden unternommen und die Unklarheiten der üblicherweise verwendeten empirischen Formeln der Unschärfe werden beseitigt und deren Beschränkungen aufgezeigt.

Резюме

Новое формулирование общей размытости в радиографии

Статья устанавливает и исследует новое формулирование общей размытости в радиографии на основании анализа функций разброса линий и краев. В общую единую формулу включены факторы размытости, вызываемой (1) экранными преобразованиями, (2) перемещением объекта и (3) геометрическими эффектами. Приводятся сравнения с экспериментами и разъясняются неопределенность и ограниченность широкоиспользуемой эмпирической формулы размытости.

References

Bouwers, A., 1936, *Fortschr. Geb. Röntgstrahl.*, **54**, 87.

Christensen, E. E., Curry, T. S., and Nunnally, J., 1972, *An Introduction to the Physics of Diagnostic Radiology* (Philadelphia: Lee and Febiger) p. 147.

Harms, A. A., 1975, in *Proc. Conf. Radiography with Neutrons, 10–11 September 1973, University of Birmingham* (British Nuclear Energy Society).

Harms, A. A., Garside, B. K., and Chan, P. S. W., 1972, *J. Appl. Phys.*, **43**, 3863.

Herz, R. H., 1969, *Photographic Action of Ionizing Radiation* (New York: Wiley–Interscience) p. 332.

Klasens, H. A., 1946, *Phil. Res. Rep.*, **1**, 2.

Newell, B. R., 1938, *Radiology*, **30**, 493.

Rossmann, K., Lubberts, G., and Cleare, H. M., 1964, *J. Opt. Soc. Am.*, **54**, 187.

Seemann, M. E., 1968, *Physical and Photographic Principles of Medical Radiography* (New York: Wiley) p. 84.

Shore, B. W., and Menzel, D. H., 1968, *Principles of Atomic Spectra* (New York: Wiley) p. 40.

Spiegler, P., and Norman, A., 1973, *Phys. Med. Biol.*, **18**, 884.